A feasibility study of a tube bundle exchanger with phase change materials: A case study

Journal of Building Engineering 78 (2023) 107622

Contents lists available at ScienceDirect

Journal of Building Engineering

journal homepage: www.elsevier.com/locate/jobe

A feasibility study of a tube bundle exchanger with phase change materials: A case study

Andrea Pignata [a], Francesco Demetrio Minuto [a,b], Andrea Lanzini [a,b], Davide Papurello [a,b,*]

[a] Department of Energy (DENERG), Politecnico di Torino, Corso Duca degli Abruzzi, 24, 10129, Turin, Italy
[b] Energy Center, Politecnico di Torino, Via Borsellino, 38, 10129, Turin, Italy

ARTICLE INFO

Keywords:
Phase change material
3D model
Latent heat thermal storage
Peak shaving
Heat transfer fluid

ABSTRACT

Latent heat thermal storage offers a flexible service to members of a heat district grid as the stored heat can be used to reduce the morning peak demand, limiting the consequences for the production facilities. This work investigates the optimized design of a latent heat thermal storage reactor, integrated in an existing building supplied by district heating, for demand-side management applications. The storage reactor was designed as a tube bundle heat exchanger in which a commercial-grade paraffin was used as the phase change material. The optimized design variables that maximized the use of the Phase Change Material were the tube pitches and the fin heights. The integration of the storage reactor with the energy system required the control and prediction of its state of charge and the power output. These parameters are usually evaluated through 3D numerical dynamic simulations that require a large computational effort, which is beyond the capability of basic microcontroller systems. A simplified parametric model has been used to overcome this issue. A load-tracking algorithm was embedded in an existing building program. The algorithm was able to reduce the thermal power peak by 62 kWh from 6:00 to 9:00 a.m. Decreasing the pitch from 95 mm to 82 mm led to a +34% increase in the use of the PCM. Similar results were obtained when the fin height was increased from 20 mm to 32 mm. The results of this investigation suggest that the proposed model could be applied to similar buildings fed by district heating network systems.

Nomenclature

cp	specific heat of the PCM (kJ/kg/K)
cp_s	specific heat of the PCM solid fraction (kJ/kg/K)
cp_l	specific heat of the PCM liquid fraction (kJ/kg/K)
cp_{ss}	specific heat of the AISI4340 stainless steel (kJ/kg/K)
F	Force field
k	average thermal conductivity (W/m/K)
k_s	thermal conductivity of the PCM solid fraction (W/m/K)
k_l	thermal conductivity of the PCM liquid fraction (W/m/K)

* Corresponding author. Department of Energy (DENERG), Politecnico di Torino, Corso Duca degli Abruzzi, 24, 10129, Turin, Italy.
E-mail address: davide.papurello@polito.it (D. Papurello).

https://doi.org/10.1016/j.jobe.2023.107622
Received 2 May 2023; Received in revised form 7 August 2023; Accepted 18 August 2023
Available online 22 August 2023

k_{ss}	thermal conductivity of the AISI 4340 stainless steel (W/m/K)
$\dot{m}$	specific mass flow rate (kg/s)
$\dot{Q}_{HTF}$	average power output (kW)
T	temperature (°C)
Tl	PCM liquid temperature of the PCM (°C)
Ts	PCM solid temperature of the PCM (°C)
u	velocity field (m/s)
θ	melt fraction (−)
ρ_{PCM}	average density (kg/m^3)
ρ_s	density of the PCM solid fraction (kg/m^3)
ρ_l	density of the PCM liquid fraction (kg/m^3)
ρ_{ss}	density of the AISI4340 stainless steel (kg/m^3)

Abbreviations

CFD	Computational Fluid Dynamics
DH network	District Heating network
EHC	Effective Heat Capacity
FEM	Finite Element Method
H	height of the fins
HTF	Heat Transfer Fluid
l	liquid fraction
LHTS	Latent Heat Thermal Storage
p	pitch of the tube bundle
PCM	Phase Change Material
s	solid fraction
TES	Thermal Energy Storage

1. Introduction

Energy storage systems play a fundamental role in the energy sector. Their integration with an energy supply system makes it possible to store any excess energy and supply it later, whenever the demand exceeds the production, or to reduce the peak consumption. Storage systems can be mechanical, electrochemical, chemical, electrical or thermal [1]. Thermal storage plays a crucial role in supplying systems when surplus energy is available and needs to be stored. It is particularly important for renewable and cogeneration systems [2]. Thermal Energy Storage (TES) is constituted by three main categories: sensible, thermo-chemical, and latent heat storage [3]. Latent Heat Thermal Storage (LHTS) uses PCMs, which undergo melting or solidification when energy is exchanged with a heat transfer medium. A PCM results in a high energy storage density and near-constant operating temperature [4–7], thereby allowing a more compact design and a large range of applications, compared to a traditional sensible heat storage device. PCMs can be classified in terms of four temperature characteristics, as reported by Du et al. [8]:

- -20 °C–5 °C, cooling mode, for domestic and commercial refrigeration [9,10].
- +5 °C–40 °C, heating and cooling mode, for free cooling and air conditioning system (buildings) [11–14].
- +40 °c to 80 °C, heating mode, for solar air heater, solar domestic hot water etc [15–17].
- +80 °C–200 °C, heating mode and power generation, for on/off site waste heat recovery and for solar thermal electrical generation [18].

The main advantages of PCMs are summarized by Devaux et al. [19] and they can be expressed as follow:

- Shifting electrical consumption from peak periods to off-peak periods
- Saving energy and improving thermal comfort
- Narrowing the gap between peak and off-peak loads of electricity demand
- Continuous usage of renewable solar energy
- Reducing cooling load of air conditioning

In addition, the most updated research focused on the thermal management of Lithium ion batteries application [20–22]. Cao et al. [20] designed a nano-encapsulated PCM for the battery thermal management. They found that nonadecane microencapsulated in water were able to increase the heat transfer rate of LIBs up to 20%, the Reynolds number and the volume fraction showed a direct correlation.

PCMs have low thermal conductivity and the heat transfer process is slow, and this in turn increases the charging and discharging times. This affects feasibility studies on LHTS when its integration in a specific application with several operational constraints must be analysed. Several heat transfer enhancement techniques have been applied to LHTS systems and investigated both experimentally and numerically [1,3]. These techniques include Phase Change Material (PCM) encapsulation under different geometries (spherical,

tubular, cylindrical, and rectangular) [23], different filling materials with high thermal conductivity (metal particles, graphite, porous media, and nanoparticles) [24,25], and extended heat transfer surfaces using fins [26,27]. Moreover, an efficient design of the configuration of a heat exchanger can improve the thermal performance of the system. Numerous types of heat exchangers have been proposed to enhance the heat transfer of latent heat storage systems [28,29]. Among these, the shell and tube heat exchanger are the types that has been studied the most [22,30–33]. Few innovative studies are focused on complex configurations, such as helical/coiled/conical fins [30], compact plate/fin heat exchanger [34], and other fins geometries such as dendritic fins [35,36]. Numerical and experimental approaches have been followed to analyse how the performance of the storage system can be influenced by different geometric and operational parameters [22,37]. Liang et al. [31] performed a thorough numerical analysis of a shell-and-tube LHTS concerning the impacts of a combination of design parameters of a single tube in a PCM shell. They studied the tube length-diameter ratio, L/d_i, the PCM volume ratio, λ, and the flow conditions. They found that when they increased the L/d_i, the ratio of the effective stored energy increased, and that an optimal λ achieved the best energy storage performance. They recommended using a laminar flow for a long tube. Water turbulent flow in a PCM heat exchanger was assessed and studied by Najafabadi et al. [38]. They found that the Reynolds number has no major effect on the melting phase. Yazici et al. [32] conducted an experimental study to investigate the solidification characteristics of paraffin as a PCM with different eccentricities of the Heat Transfer Fluid (HTF) tube, and moving it up and down according to the centre of the outer shell. Their results indicate that eccentricity makes the total solidification time longer. Therefore, they suggested that the HTF tube should be geometrically concentric. Kibria et al. [39] numerically investigated the heat transfer behaviour of a storage unit with different flow parameters for the charging and discharging cycles. Their study revealed that an increase in the HTF inlet temperature and mass flow rate reduced the time required to complete the phase change of paraffin wax. Among the different heat transfer enhancement techniques, adding fins has proved to be the most feasible solution, due to their ease of manufacturing and low cost, together with their high efficiency [40]. Different types of fins have been studied extensively, including such geometrical solutions as radial fins [41–44] and longitudinal ones [33,45–48]. Agyenim et al. [49] conducted an experimental study to compare heat transfer enhancement using circular or longitudinal fins with a control system without fins. The authors found that only the longitudinal finned system achieved complete melting for an imposed 8 h charge, and it also provided a more uniform heat distribution. The dynamic behaviour of an LHTS unit is commonly addressed using numerical models capable of describing the physical complexity of the phase change phenomenon. A numerical approach allows a design to be optimized by varying different parameters, thereby avoiding expensive experiments. Hosseini et al. [48] studied the effect of longitudinal fins in a double-pipe heat exchanger during the charging process. Their three-dimensional numerical model described the melting behaviour of the PCM. They observed that the presence of high fins provided a more symmetric melting and led to a better absorption of the energy, thereby improving the thermal conditions of the system. Niyas et al. [50] developed a 3D model, using commercial software based on a finite element scheme, to determine the optimal number of HTF tubes and longitudinal fins for each tube that provided the fastest discharging time. Abreha et al. [51] examined the effects of an HTF mass flow rate and temperature variations on the melting behaviour and observed such performance parameters as the charging time, liquid fraction, average transient temperature, and stored energy for a multiple-finned HTF tube design. Khan et al. [52] used a 2D finite element computational model to perform a parametric investigation on the number and orientation of tube passes, the longitudinal length and thickness of the fin, and inlet temperature of the HTF. They observed that the longitudinal length of the fin has a greater impact on the melting rate than the fin thickness. Sciacovelli et al. [36] proposed the optimization of Y-shaped fins with a single and double bifurcation. A 2D cross-section conduction-based model was implemented to evaluate the complete solidification of paraffin wax over a short- and a long-time interval. Numerous studies have investigated the optimization of the thermal performance of latent heat storage in search of the best charge/discharge time by observing the influence of a variety of operating parameters, such as the HTF inlet temperature and flow rate. However, in many practical applications, it is necessary to optimize the system with design and operational constraints pertaining to the integration of the LHTS in an existing heating system. Agyenim and Hewitt [53] investigated the implications of integrating a PCM storage system with an air source heat pump to meet the daily heating energy load of residential buildings in the UK. Their study evidenced the influence of the HTF inlet temperature on the specified testing time interval. Nallusamy and Velray [54] developed a simulation model in which they considered the effect of the dynamic outlet temperature on the solar thermal collector connected to the LHTS. Li et al. [55] analysed the effect of different water mass flow rates on inlet and outlet temperature variations, the charging time, and the total energy in different heat storage energy systems. Xu et al. [56] studied the performance of an LHTS unit integrated in a residential heating system with a variable HTF flow rate profile (constant, linear increasing, and parabolic increasing) imposed as an inlet condition to stabilize radiators. Sciacovelli et al. [57] proposed dynamically controlling the LHTS through a non-steady-state HTF mass flow rate with a quadratic equation to limit outlet temperature variations during the discharging process. The optimization of a control strategy in energy systems requires a dynamic simulation of the storage of thermal latent heat at a system level. Nevertheless, the studies conducted so far have only referred to a predefined time profile of the HTF inlet temperature [54] and flow rate [56] as the LHTS inlet boundary condition. In addition, only a few studies have analysed the behaviour of a system and included the operational constraints of the application, such as the thermal power output profile, under transient charge/discharge conditions [58]. It can be inferred, from the published studies, that the definition of the operating parameters is crucial for the optimal integration of LHTS in energy systems. Therefore, more attention should be paid to the analysis of the operating conditions of LHTS and to how such a system should be defined to satisfy the heating needs of a specific application. The authors have proposed a load tracking algorithm in this framework. The proposed algorithm was used for a shell and tube LHTS with longitudinal fins attached to the outer surface of the tube to improve the heat transfer in the PCM that filled the shell. The algorithm can identify the working points of the system during the discharge process. The study variables are the flow rate, the inlet HTF, the outlet temperature, and the heat output required by the user. The design phase of the storage unit dealt in this work, introduces a methodology that takes into account the operational constraints imposed by the application under consideration, which, in this case, refers to the integration of the LHTS in the district heating

network. The results of this research enhance our understanding of LHTS systems with commercial PCM, optimized in terms of the geometrical and structural reactor design, for peak shaving in an existing building: the Energy Center of Turin, Italy. The optimization of a thermal storage reactor has been studied, considering the constraints, to increase its compactness, by ensuring complete solidification in the PCM discharge phase. The main operational constraint resulted to be the solidification time. The obtained configuration was used inside a real building in Turin. The proposed control strategy was applied to modulate the load of an LHTS to reduce the peak thermal power required by the district heating network. The goal of this study was to simulate the PCM discharge phase using the aforementioned load tracking algorithm with a variable HTF input flow rate to satisfy the thermal power demand.

2. Material and methods

This section begins with a comprehensive description of the design approach that we used. Moreover, it also details the modeling of the LHTS constraints and the subsequent optimization of the design. This is followed by description of the numerical simulation model, in which the underlying assumptions, the employed governing equations, and the steps taken to create a 2D multitube cross-section are presented in detail. The mesh generation method and an in-depth explanation of the investigated parameters are also provided. Finally, we introduced an LHTS concentrated parameter model, i.e., a Load Tracking Algorithm, which we designed to reproduce the results of the numerical simulations while significantly reducing the computational load, see Fig. 1.

2.1. Design approach

This paragraph introduces the constraints and design choices introduced to optimize the LHTS unit to handle the thermal demand required by the heating system of the considered building. Practical application constraints, such as a thermal load profile and the temperature range were considered.

2.1.1. Application constraints

The considered practical application constraints refer to the thermal load profile and temperature range. The approach to designing an LHTS in a building heating system supplied by a district heating network should consider the operational variables of the user's thermal load and the temperature operating range. The daily operations of a district heating system are characterized by a typical peak in the thermal request in the morning while, in the afternoon, the thermal load shows a quasi-steady-state profile, see Fig. 2 [59]. An interesting strategy to improve the operational management of a District Heating (DH) network at the building level is to reduce the morning peak using an LHTS device that can release the thermal power required by the user over a limited period.

Therefore, the first application constraint required defining a fixed time interval for the discharging operation to satisfy the user's thermal need in that time range. The temperature application range affects the selection of the PCM, which should have a suitable phase change temperature. When the LHTS is installed between the primary district heating network and the secondary circuit (building side), the phase change temperature, T_{pc} should be selected between the supply temperature T_{supply} and the demand temperature T_{demand}. Thus, the following inequality should be respected:

$$T_{supply} \geq T_{pc} \geq T_{demand} \tag{1}$$

T_{supply} is obtained from the primary district heating network, which works over the 65–120 °C temperature range to charge the storage with the heat delivered from the primary source. T_{demand} is obtained from the building heating network and depends on the terminal device (radiators, radiant floor/ceiling, etc.) chosen to be connected to the storage unit for the discharging operation. Furthermore, the temperature range also determines the operating conditions of the HTF, regarding the water inlet and outlet temperatures involved in the LHTS.

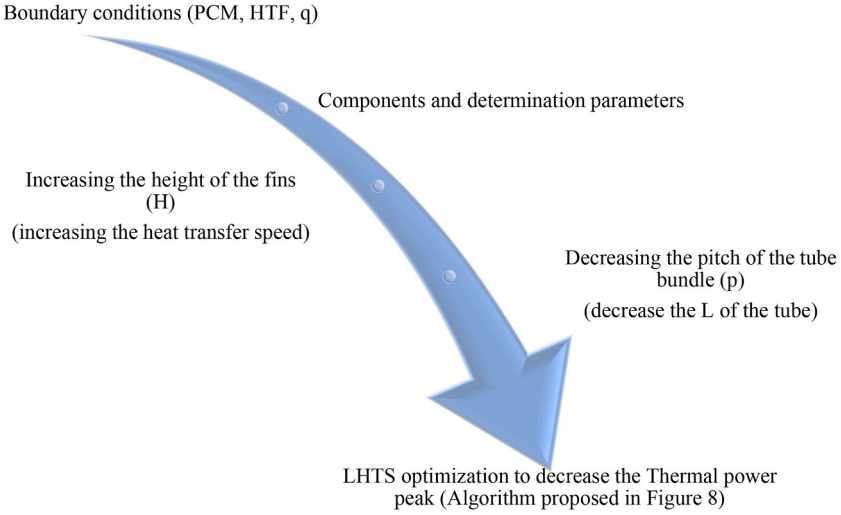

Fig. 1. Schematic representation of the proposed methodology.

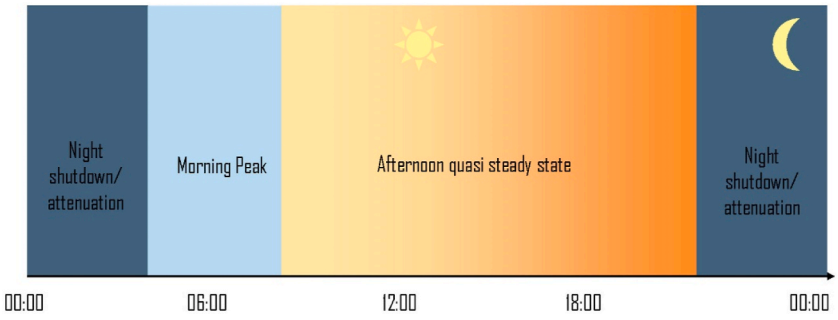

Fig. 2. Typical operations of a district heating network [59].

2.1.2. Optimization of the LHTS unit

The performances of an LHTS are imposed by the thermal user and depend on the integration of the system which, as an operational constraint, needs thermal energy to be supplied at a given temperature for a defined time, thereby limiting the time necessary for the complete solidification of the PCM. This issue was addressed by modifying the design of the shell and tube system to optimize the amount of phase change material involved in the thermal exchange, and this resulted in a more compact and efficient storage unit. The performed optimization allowed the amount of PCM that did not contribute to the latent heat exchange to be removed. The amount of PCM that did not solidify in a shell and tube LHTS, where the PCM filled the shell and the tubes were equipped with longitudinal fins, was in regions of the shell far from the fluid-tube-PCM interface, where the heat transfer was faster than in the outer regions (i.e., in the middle of the tube). The approach adopted for this analysis consists of two design choices:

1. Decreasing the pitch of the tube bundle *(p)*
2. Increasing the height of the fins *(H)*

The two solutions offer an opportunity to maximize the utilization of the PCM and result in the reduction of the entire volume due to a decrease in the tube length (solution 1) or an increase in the penetration of the fins, which speeds up the heat transfer (solution 2). In addition, a design optimization, aimed at maximizing the phase-changing material that completes the transition process, reduces the costs of the system. This is relevant in applications where the time necessary to discharge the system is constrained and there would therefore be an unused amount of PCM during the storage operations. Thus, this portion of PCM would result in an excessive cost that should be avoided.

2.2. Numerical FEM-CFD simulation

The transient behaviour of the latent heat storage unit has been studied. The thermodynamic performance was determined using Finite Element Method (FEM) numerical models and the CFD approach, developed through COMSOL Multiphysics 5.2 software, whose characteristics allow several coupled physical phenomena to be studied. In the specific study, the numerical model aimed to describe the transient behaviour of the system under different heat transfer mechanisms and fluid-dynamic conditions: latent heat exchange in the PCM, conduction through the finned surfaces, and forced convection inside the heat transfer fluid. The study of the thermal transient of the storage unit was only performed for the discharge phase. This, as has been demonstrated in numerous studies over several years [50,60,61], allows the effects of natural convection to be neglected. The dominant phenomenon in the solidification process is thermal conduction. The thermal model was therefore based on this main hypothesis.

2.2.1. Computational domain and model assumption

The structure of the system under study required the description of the physical phenomena in both the radial and longitudinal directions [49]. This involved first analysing the phase change evolution process of the PCM and then studying the forced convection along the entire length of the duct. The geometry, therefore, had to be three-dimensional. However, a simplification of the model was made by taking advantage of reduced geometries obtained as a result of the presence of symmetries or parts of the unit that were repeated in the whole structure of the storage device.

The component consists of a tube bundle exchanger in which the materials, and the physical and geometric properties of the ducts, inserted inside a cylindrical casing, are identical. Thus, this simplifies the system as a repetition of a single element consisting of a single finned tube surrounded by a certain amount of PCM. The latter makes up a concentric “fictitious” external cylinder of the single pipe, thereby determining the “elementary module” presented in Fig. 3.

The radius of the outer cylinder was obtained by considering half the pitch between two pipes. A further simplification of the geometry of the elementary module was determined. A homogeneous distribution was identified along the duct diameter by observing the cross-section in Fig. 3. This assumption allowed the object of study to be reduced to only 1/8 of the cylinder, as depicted in three dimensions in Fig. 4. The obtained circular sector is repeated symmetrically to the radius of the circle drawn for every 45°.

The introduced geometric simplifications only define the computational domain used to perform the numerical simulation of the component.

Moreover, the following physical assumptions were adopted to describe the heat exchange and the fluid motion:

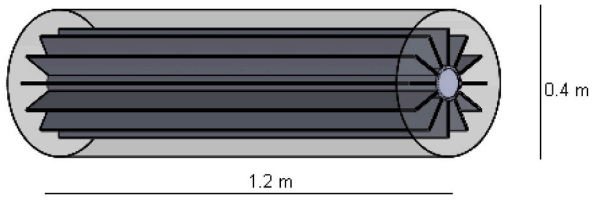

Fig. 3. Elementary module of a multi-tube LHTS unit.

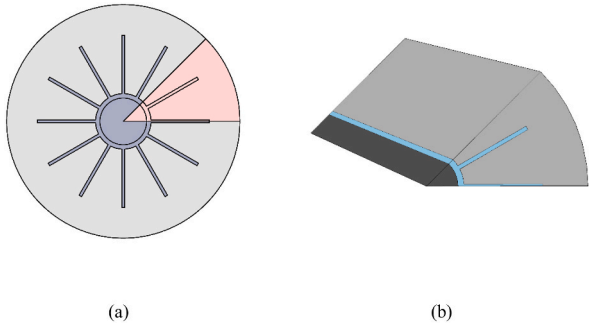

Fig. 4. 2D Cross-section of the elementary module (a) and 3D representation of the computation domain (b). Light blue is used to indicate stainless steel, while gray is used to show the PCM. (For interpretation of the references to colour in this figure legend, the reader is referred to the Web version of this article.)

- A phase change transition occurs in a finite temperature interval.
- PCM is homogeneous and isotropic.
- HTF is incompressible.
- The HTF properties are constant with the temperature.
- A laminar and fully developed flow takes place (Re $<$ 2000 [62]).
- The viscous dissipations in the fluid flow are negligible.

2.2.2. Governing equations

The physics that had to be solved in the numerical model were developed using a conjugated heat transfer. The most challenging aspect of modelling the behaviour of the PCM was incorporating the latent heat effect released from the material during the solidification process inside the numerical model. This issue was addressed by modifying the definition of the specific heat of the PCM, and by introducing a term defined as "*effective heat capacity*" (EHC) [63–65]. The heat capacity of the PCM was modified as shown in Eq. (1), and the EHC was expressed by Eq. (2). The obtained function was inserted into the COMSOL Multiphysics software using a piecewise function with a continuous derivative [66].

$$\theta = \begin{cases} 0 & \\ \dfrac{T - T_S}{T_L - T_S} & for \quad T_S \le T \le T_L \\ 1 & \end{cases} \qquad (2)$$

The phase change occurs over a defined temperature range, and problems of this type are known as mushy region problems. The boundaries of this range are defined by the solid and liquid temperatures, expressed as $T_{pc} - \Delta T/2$ and $T_{pc} + \Delta T/2$, respectively. The phase of the substance was defined within this range. The function that expresses the melt fraction is θ which is in Eq. (2). This term was used to modify the specific heat capacity, the density and the thermal conductivity of the PCM, see Eqs. (3)–(6).

$$c_p = \begin{cases} c_{ps} & for \quad T < T_S \\ c_{p,EFF} & for \quad T_S \le T \le T_L \\ c_{pl} & for \quad T > T_L \end{cases} \qquad (3)$$

$$c_{p,EFF} = \frac{c_{ps} + c_{pl}}{2} + \frac{L}{T_L - T_S} \qquad (4)$$

$$\rho = \rho_s(1 - \theta) + \rho_l \qquad (5)$$

$$k = k_s(1 - \theta) + k_l \qquad (6)$$

The absence of a natural convection effect in the model meant the heat transfer equation could be considered the same as when in a

solid medium, that is, by disabling the velocity component. Eq. (7) describes the heat diffusion by conduction that occurs in both the PCM and in the finned tubes, together with their thermo-physical properties.

$$\rho c_p \frac{\partial T}{\partial t} = k\nabla^2 T \tag{7}$$

The fluid dynamics was described through the solution to the Navier-Stokes equations, albeit only for the HTF domain. Under the assumption of an incompressible and fully developed fluid, the motion was considered stationary, and the continuity and the momentum equations were Eq. (8) and Eq. (9). In this way, the physics of the fluid was described in a segregated approach, first by solving the fluid dynamic problem and then the thermal problem through Eq. (10). The latter equation received the velocity field obtained previously from the Navier-Stokes equations.

$$\nabla \cdot \boldsymbol{u} = 0 \tag{8}$$

$$\rho(\boldsymbol{u} \cdot \nabla \boldsymbol{u}) = -\nabla p \boldsymbol{I} + \mu \nabla^2 u + \boldsymbol{F} \tag{9}$$

$$\rho c_p \frac{\partial T}{\partial t} + \rho c_p \mathbf{u} \cdot \nabla T = k\nabla^2 T \tag{10}$$

2.2.3. 2D multitube cross-section

The two-dimensional section of the model has been obtained with a horizontal cutting plane at the outlet section of the heat exchanger. This model was used to analyse the effects of the different tubes on the behaviour of the PCM. The 2D model is similar to the three-dimensional one. The physical assumptions and the governing equations are analogous, as previously described, with the only difference being that the computational domain of the fluid domain is no longer considered. Therefore, the transient simulation only concerns the thermodynamic side, and the fluid behaviour is not studied. Thus, the velocity terms disappear from Eq. (9), and not the Navier-Stokes equations are used. This approach did not affect the integrity of the physical problem, which was respected by introducing a new boundary condition. The Dirichlet boundary condition was imposed at the inner wall of the heat transfer tubes by assigning the HTF temperature, i.e., the temperature of the inner tube surface, and the time evolution obtained from the 3D model simulation, which was explained in the previous section. Fig. 5 illustrates the simplified geometry of the 2D model. In this case, the reference domain is a hexagon that corresponds to the minimum subdivision of the tube bundle characterized by a staggered arrangement.

The scope of this type of result visualization is to observe the behaviour of the PCM in the most critical region, that is, the outlet section where the fluid exits and completes the heat transportation. Moreover, the contribution of the fin height can be appreciated more from a 2D view, in terms of thermal conductivity enhancement.

2.2.4. Mesh generation

The mesh of the 3D model has been obtained by extrusion along the longitudinal direction of the triangular elements defined on the front surface, called the source surface, to create a series of hexahedral elements that occupy the entire volume of the component. The whole meshed component is shown in Fig. 6.

This approach can be considered reasonable, given the geometry under study, which is characterized by the development of the

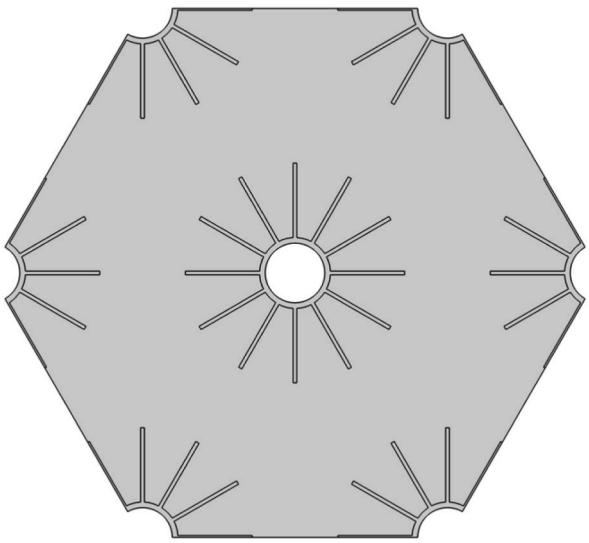

Fig. 5. 2D computational domain of a staggered tube bundle heat exchanger.

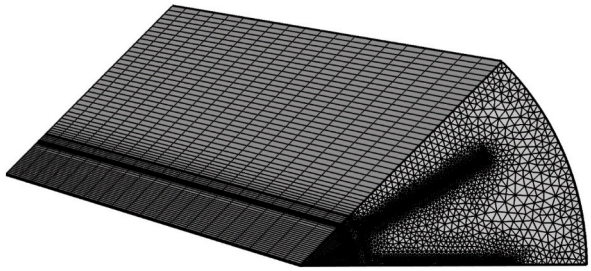

Fig. 6. Meshed model of the component.

front section in the longitudinal direction. Moreover, it avoids unnecessary high computational times, due to the large number of grid elements. Special meshing features of COMSOL Multiphysics were used, such as boundary layers for the fluid wall interface, element distribution, and a finer size in the critical region of the component, where the thermal gradients were more pronounced, along with the contact layer of different materials and the HTF inlet/outlet.

2.2.5. Investigated parameters

The dynamic response of the latent storage unit has been analysed using the developed numerical model, which was implemented in the COMSOL Multiphysics simulation platform through which it was possible to obtain the system evaluation parameters. The main parameters resulting from the simulations are listed below.

- HTF outlet temperature *(T_{out}), is* calculated as the mean surface temperature of the outlet section of the tube in the fluid domain.
- Melt fraction *(θ),* calculated with Eq. (4) as an average of the PCM volume.
- Average power output, as in Eq. (11) below.

$$\dot{Q}_{HTF} = \dot{m} c_p (T_{out} - T_{inlet}) \tag{11}$$

Each of the above-mentioned parameters is a function of time and is provided by the numerical model as a temporal evolution.

2.3. Concentrated parameter model

The integration of latent thermal storage in heating systems requires a thorough evaluation of the different operating conditions to meet the desired thermal profiles. To facilitate this process, it would be beneficial to have a tool that can quickly identify different working points of the system, and which can easily be integrated with thermal load monitoring devices within the thermal circuit of the application. For this reason, we have proposed a Load Tracking Algorithm to offer a control strategy that can modulate the operations of the latent thermal storage system. The goal of the load tracking algorithm is to develop a concentrated parameter model that can describe the dynamic behaviour of the storage system under load modulations, while keeping the computational requirements low, compared to when a complex simulation software, such as COMSOL, is used. The load modulation of the LHTS refers to the variation of the operating conditions represented by the inlet flow rate of the HTF. The load tracking algorithm identifies an appropriate inlet flow rate profile to obtain a thermal power output profile that meets the thermal demand required by the users. Hence, the LHTS becomes flexible and adjustable, according to the heat demand, and the proposed model helps to optimize the integration and management of the storage unit in practical applications. Moreover, the proposed methodology avoids the need for complex and robust thermo-fluid dynamics simulations, as described in the previous sections, which, in this case, would require a time-variant velocity field at each stage of the transient model. However, a numerical simulation model is useful for constructing parametric curves that indicate the performance of the LHTS for different fluid flow rates kept constant over the thermal transient. Once the curves of different input flow rate values have been obtained, the algorithm identifies the operating conditions (working points) of the LHTS on these curves according to the user's thermal power request. The obtained reference curves are grouped into two maps and could be described as follows:

- MAP1 explains the operating window of the storage, in terms of HTF outlet temperature and output thermal power, for different flow rates. It permits the reference load curve to be individuated when a specific thermal power is required and the HTF leaves the storage at a certain temperature.
- MAP2 explains how the HTF outlet temperature changes in time, depending on the operating conditions. It provides the thermal response of the LHTS when the fluid flows at a given flow rate for a defined time step.

The algorithm was developed by writing a MATLAB® R2020a code that works cyclically for each value of the thermal load profile. The MAP1 and MAP2 curves are expressed in a discrete domain, as they are the outputs of a numerical model based on FEM.

The reference thermodynamic behaviour of the PCM-TES needed to be evaluated for different load conditions to obtain the curves related to the evolution of the HTF outlet temperature and to establish the relationship between the latter and the output thermal power. The simulations were performed by changing the inlet flow rate of the heat transfer fluid. The chosen geometry and fluid-dynamic conditions of the storage were assumed to be able to handle about 1.98 m^3/h of the water, which corresponds to the maximum load (100%), at an inlet velocity of 0.024 m/s. Simulations with different flow rates, from 0.024 m/s (100%) to 0.002 m/s (10%), were performed. The results of each simulation are illustrated in Fig. 7, where MAP1 on the left represents the linear

dependence of the output thermal power on the HTF outlet temperature, while MAP2 on the right shows the temperature evolution of the fluid. As expected, the increase in the velocity of the fluid improves the heat exchange with the highest thermal power (high-dark gray line on the left), with the same inlet temperature of 25 °C for all the simulations. The considered high flow-rate condition increases forced convection. This behaviour can be explained by considering the temperature evolution (Fig. 7 on the right), which decreases more rapidly as the velocity of the fluid increases (from LOAD 10% to LOAD 100%).

Moreover, each curve is defined with a corresponding function to perform the algorithm calculations. The linearity depicted in MAP1 is maintained by the linear interpolation function $f_{MAP1,i}(T)$, which provides the thermal power according to the temperature of the fluid. The MAP2 curves, instead, are expressed with a discrete function, $f_{MAP2,i}(t)$, where the discrete-time domain is defined with a discretization step of 10 s, from 0s to 10800s.

2.3.1. Control strategy algorithm

The main features of the algorithm are summarized hereafter, together with a description of the input parameters, the performed calculations, and the outputs of the model. The algorithm operates cyclically and performs a series of calculations for each thermal power value obtained as an input parameter, which represents a single point *k* of the user's thermal profile that has to be satisfied. Therefore, the operations carried out by the algorithm for a *k-th* cycle for each power value that constitutes the thermal profile required by the user are as follows:

1. Step 1: Localizing working point *k* on MAP1 as temperature and power coordinates. The temperature is the HTF outlet temperature, T^k, and it is determined for each cycle by moving within MAP2, although the value is only known for the first cycle (k = 0), and it is the initial temperature value that is assumed as the initial conditions when the discharging process starts. The power is the external input, $q^{in,k}$, and it is taken from the user thermal demand profile.
2. Step 2: Identifying the load curve closest to the working point individuated in step1. The identified curve, *i*, refers to a given flow rate of the fluid, and the corresponding value of the input fluid velocity, u_i^k, is thus obtained.
3. Step 3: Determining the new HTF outlet temperature value using MAP2, by moving along curve *i* identified in step2 from point A, relative to temperature T_i^k, to point B, which indicates the temperature of the fluid, T_i^{k+1}, after Δt seconds. Hence, the thermal response of the PCM on the fluid temperature is evaluated as:

$$T_i^{k+1} = f_{MAP2,i}(t + \Delta t) \tag{12}$$

where Δt corresponds to the time resolution of the user thermal power profile (i.e., in a 15min time profile $\Delta t = 900s$).

4. Step 4: Calculating the thermal power $q^{out,k}$ exported from the water through Eq. (10), using T_i^{k+1} calculated in the previous step

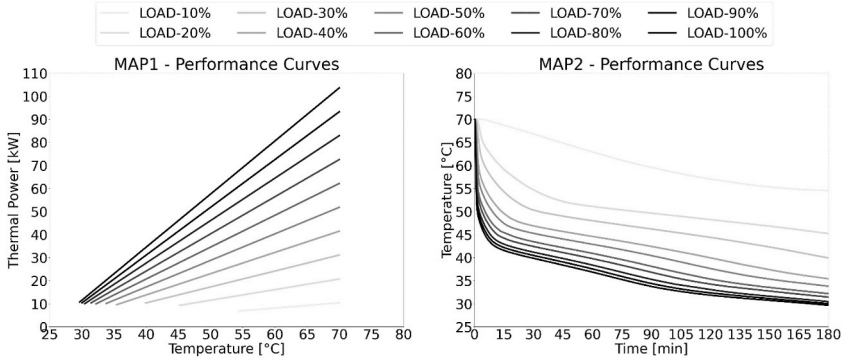

Fig. 7. Performance curves for different fluid flow rates: LOAD 100% = 1.98 m^3/h, LOAD 10% = 0.2 m^3/h.

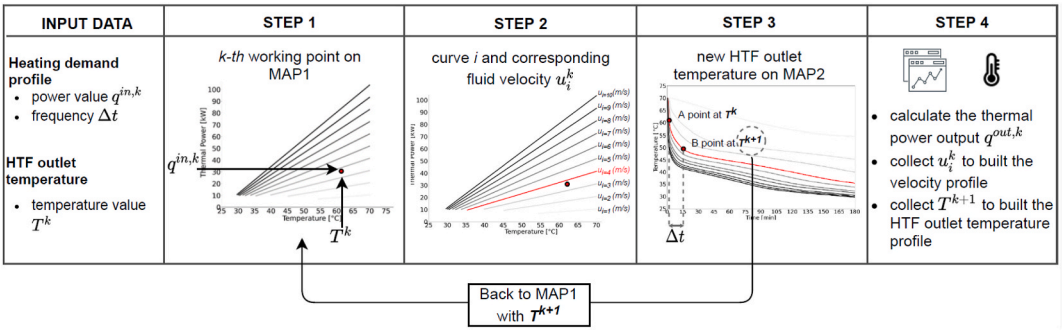

Fig. 8. Graphical representation of the algorithm calculation process for each k-th cycle.

as the outlet temperature. The fluid velocity, u_i^k, identified in step 2, is used to evaluate the fluid flow rate. The inlet temperature is kept constant and does not vary at each iteration.

At this point, the calculation cycle starts again, from step 1, and introduces the new thermal power value, $q^{in,k+1}$, required by the user, as well as the temperature value of the fluid T_i^{k+1} calculated in step 3. The process that the algorithm carries out for each *k-th* cycle is graphically represented in Fig. 8.

At the end, when all the required thermal power values have been processed, the model outputs three profiles consisting of all the LHTS working points identified at each cycle. The obtained profiles are:

- The HTF inlet velocity profile *u(t),* which collects all the u_i^k values;
- The HTF output temperature profile $T^{out}(t)$, which collects all the T_i^k values;
- The thermal power profile is delivered by LHTS $q^{out}(t)$, which collects all the $q^{out,k}$ values.

However, it should be emphasized that the algorithm does not perform thermodynamic calculations, and that the obtained profiles are characterized by a set of working points under different thermodynamic conditions that have already been simulated. For this reason, and to verify the consistency of the thermal behaviour of the system, the obtained profiles were compared with those resulting from the numerical 3D model in COMSOL, where the thermofluidynamic evolution of the system is considered. A numerical simulation was implemented by introducing the HTF inlet velocity profile, *u(t),* obtained by the algorithm as input, and the results obtained on the HTF outlet temperature profile were observed.

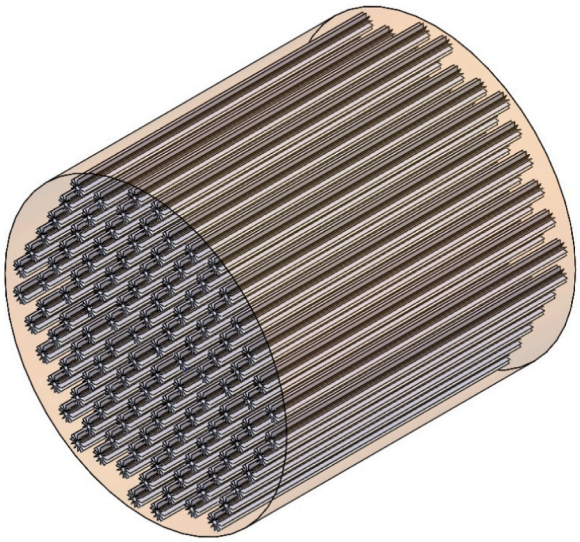

Fig. 9. 3D view of the heat exchanger device.

Table 1
Thermophysical properties of PureTemp53 [67].

Melting temperature - T_{pc} (°C)	53
Transition range - ΔT (°C)	5
Latent heat - L (kJ/kg)	225
Thermal conductivity (solid) - k_s (W/mK)	0.25
Thermal conductivity (liquid) - kl (W/mK)	0.15
Density (solid) - ρ_s (kg/m^3)	920
Density (liquid) - ρ_l (kg/m^3)	840
Specific heat (solid) - c_{ps} (kJ/kgK)	2.36
Specific heat (liquid) - c_{pl} (kJ/kgK)	2.60

Table 2
Thermophysical properties of AISI 4340 stainless steel.

Thermal conductivity - k_{ss} (W/mK)	44.5
Density - ρ_{ss} (kg/m^3)	7850
Specific heat – $c_{p,ss}$ (kJ/kgK)	0.475

3. Results and discussion

3.1. LHTS unit

The PCM storage unit was designed as a cylindrical tube bundle heat exchanger, in which the phase change material fills the shell side, while the heat transfer fluid flows inside the longitudinal finned tubes. The heat released from the PCM during the discharging phase permits the carrier fluid, water in this case, to be heated. A portion of the heat exchanger can be observed in Fig. 9, in a 3D representation.

The geometry of the storage unit is characterized by a heat exchanger containing 112 tubes of a length of 1,2 m, a diameter of 16 mm, and a tube thickness of 2 mm. There are 12 fins of 20 mm in height and 1 mm in thickness in each tube. The adoption of this kind of fin permits a 10 times higher increase to be obtained in the heat exchange surface than smooth tubes without fins. The tube is arranged in a staggered way and the pitch is 95 mm. The PCM is a bio-organic material, that is, *PureTemp53* [67]. The melting temperature of the PCM is 53 °C, and it has a transition range of 5°. The PCM appears as a wax in its solid state, while it appears as a clear liquid at a temperature above the transition one. Its bio-organic nature makes it compatible with the materials that make up the system (i.e. tubes, fins, and external containment casing) in terms of corrosivity, as well as chemical and thermal stability, thereby guaranteeing over 1000 operation cycles [67]. The thermo-physical properties of *PureTemp53* are listed in Table 1.

The tubes and the longitudinal fins are in stainless steel (AISI 4340), the properties of which are provided in Table 2. The issue related to the poor thermal conductivity of PCM was tackled by inserting a steel material with a thermal conductivity of about 200 times higher than the PCM.

3.2. Boundary conditions and initial values

The numerical model developed to describe the thermal behaviour of LHTS is characterized by the following assumptions concerning the CFD boundary conditions and initial values. Initially $(t = 0)$, the HTF domain is given zero velocity (no flow condition), and all the domains (PCM, HTF, and inner tube) are given a constant higher temperature of $T(t = 0)$ during the discharging process, that is, a value of 70 °C. The inlet of the HTF tubes is given a constant lower temperature of T_{inlet} and a constant fluid velocity of 0.024 m/s at any time $(t > 0)$. The inlet temperature is set at 25 °C. All the outer surfaces are given adiabatic conditions to avoid heat losses to the ambient, and symmetry conditions to account for the geometry reduction, thus keeping the physics of the problem valid. A non-slip boundary condition was introduced to account for the zero velocity on the HTF tube walls, while negligible temperature gradients were incorporated in the normal direction near the HTF outlet, the convective flow normal to the outlet surface was eliminated, and an outflow boundary condition was considered.

3.3. Integration of LHTS in district heating

The LHTS unit was applied, at the building level, to a thermal energy network supplied by a district heating substation. The PCM storage was hypothesized to be integrated into the technical building system with the scope of reducing the peak-load of the thermal power consumption that occurs in the morning, as shown in Fig. 10. This refers to the heating demand for the space heating of an office building located in the city of Turin, which is part of climatic zone E, and the heating season covers a period from October 15th to April 15th. Fig. 10 illustrates a typical daily load profile with a 15-min resolution, which was individuated using a clustering technique on the measured data of the entire heating season [68].

During the heating season, the unit was programmed to anticipate the start-up of the heating plants in the building, which were set up to operate from 07:30 to 19:30 on working days, at an hour and a half in advance, due to the drop in water temperature of the plants from the 35 °C set-point temperature of the radiant floor panels to 25 °C. An application of the previously described and analysed thermal storage device was studied. The storage system was designed to release the thermal energy required by the radiant floor panels over a defined time interval from 06:00 to 09:00. Therefore, the useful time for the solidification of the PCM and the release of thermal energy to the water that circulates in the system, was 3 h. In this period, the PCM carried out the solidification process while releasing

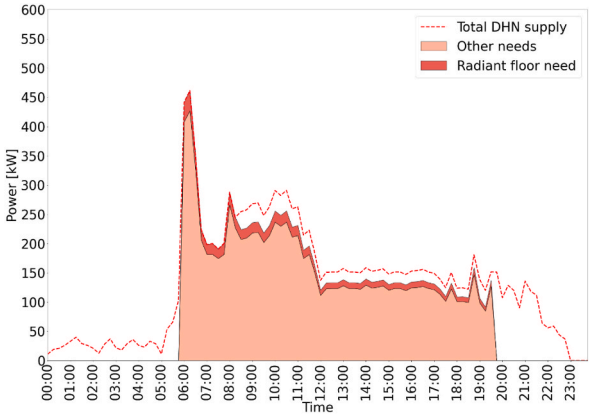

Fig. 10. Building the heating demand (time division 15-min).

the latent heat to the water, as HTF, to raise the temperature of the water that fed the radiant panel circuit, with the consequent challenge of tracking the thermal power profile of the user, as highlighted in Fig. 11.

Regarding the operating temperatures, the latent heat storage technology required a reasonable range of temperatures. This range was limited by the supply temperature and the demand temperature within which the transition temperature of the PCM should have been (see Section 2.1.1). This range guarantees the unidirectional thermal flow that can be exchanged in the charging and discharging phases [60]. The charging phase of the PCM storage was assumed to occur after 19:30, when the heating system switched off but thermal energy from the district heating was still available, as can be seen in Fig. 10. Thus, it was hypothesized that the storage received heat through hot water from the district heating primary circuit at 90 °C, that is, at the supply temperature, and it was also assumed that, at the end of the melting process, the final temperature of the PCM reached 70 °C. The latter temperature corresponds to the initial value of the temperature implemented in the numerical model to simulate the discharging process. The temperature range considered for the application was suitable for the selected PCM, which had a phase change temperature of 53 °C, while the supply temperature from the district heating primary circuit was 90 °C and the target demand temperature value required by the radiant floor panels in the building heating network was set to 35 °C.

3.4. Grid independence

A grid-independent test was carried out by varying the size of the elements and the number of extrusion levels along the longitudinal direction of the triangular elements that had been defined on the front surface (source surface) of the 3D model. Fig. 12 illustrates the evolution of the HTF outlet temperature, which was stopped at 100 s. Grid convergence was reached when 88,180 elements provided the same results as 176,360 elements. Thus, the maximum and minimum sizes of the 60 mm and 0.32 mm elements with 20 distributed extrusion levels were found to be sufficient to ensure grid-independent results. The mesh results of the 2D cross-section simulation are only those that were obtained on the source surface and the dimensions of the elements are those related to the grid independence condition, albeit resized according to the dimensions of the new geometry.

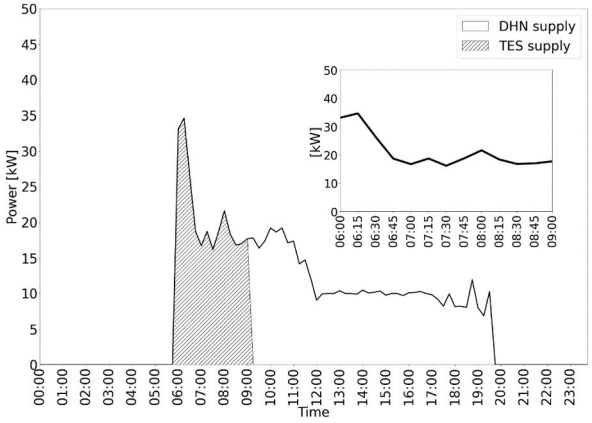

Fig. 11. Thermal profile required for the radiant panels to be satisfied using the LHTS discharge.

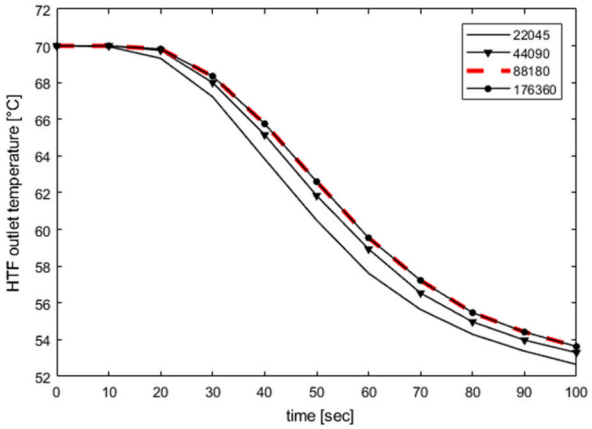

Fig. 12. Grid independence study results.

3.5. Optimization of the solidified PCM

Two solutions were proposed to optimize the solidification of the PCM over the 3 h of the discharging process, and the numerical model was used to compare the performance of the selected systems, that is, models with 95, 90, 85, 82 mm of pitch *(p)* and 20 mm of fin height for all the considered cases, and models with 95 mm of tube pitch and 20, 24, 28, 32 mm of fin height *(H)* for all the cases. The number of HTF tubes was changed in the second solution model to maintain the same PCM volume between the two solutions and the same heat transfer surface. This approach allowed only the effects of the heat transfer to the PCM regions to be evaluated. The optimization was based on the melt-fraction value obtained at the end of the process, which was calculated, with Eq. (3), as the average volume, while the average thermal power output was also observed and a comparison of the values is given in Table 3 and Table 4.

It can be seen from Table 3, concerning the pitch optimization, that a reduction in the average thermal output occurred with a drop of −2.7%, compared with the starting configuration (p = 95 mm; H = 20 mm). This is justified by the reduction of −27.2% of the amount of PCM, which was the energy source considered for the release of thermal energy. The removal of the PCM led to a −90.9% reduction in the material which, at the end of the 3 h of discharge, had not contributed to the latent heat exchange. An increase of +34% in energy resource exploitation, related to the larger amount of solidified PCM, was also observed. In addition, by reducing the length of the tube, a more compact LHTS than the base case solution with 95 mm of pitch was obtained. The results obtained after an increase in fin height are provided in Table 4. In this case, the average thermal power output is slightly increased, that is, by +3.3%, because the penetration of highly conductive material in the PCM determined a flatter behaviour of the HTF outlet temperature, as illustrated in Fig. 13b on the right. In this case, the increase in the exploitation of the stored energy reached +33% and the same PCM remotion as before. However, in this case, the volume of the steel increased by +6.47%, which led to an increase in costs, but this could be offset by the large reduction in the amount of PCM, which would result in an extra cost if this amount were not used in the heat exchange. It is important to note that, for both optimizations, the variation in the average thermal power was contained, compared to the initial configuration (± 3%) for the benefit of the full use of PCM (98%). Therefore, the sizing of an LHTS to maximize the PCM used for discharge purposes does not affect the thermal power delivered by the system to any great extent and makes the system more compact and efficient. The HTF outlet temperature is illustrated in Fig. 13 for the various models of the two optimizations. The temperature evolution on the left for optimization 1 shows very small differences between the curves of each pitch value. It is interesting to note the first instants (0–30 s) of the discharging process, where the new fluid starts to flow, and the old fluid starts to leave the tube bundle. Here, the process to remove the initial fluid is fast and appreciable, and it shows an almost constant temperature. Then, as the discharging process continues, the temperature drops rapidly for the first 3–5 min until the latent heat exchange becomes dominant. This process can be observed from the sharp change in the slope of the curves. Moreover, the temperature always decreases

Table 3
Optimization of the pitch.

Pitch p (mm)	PCM Volume (m^3)	Average Thermal Power $\dot{Q}_{HTF}$ (kW)	PCM - solidified (%)
95	0.88	23.69	73.28
90	0.78	23.52	83.22
85	0.69	23.27	93.37
82	0.64	23.06	97.56

Table 4
Optimization of fin height.

Fin height H (mm)	PCM Volume (m^3)	Average Thermal Power $\dot{Q}_{HTF}$ (kW)	PCM - solidified (%)
20	0.88	23.69	73.28
24	0.78	23.94	83.60
28	0.69	24.17	92.47
32	0.64	24.42	97.52

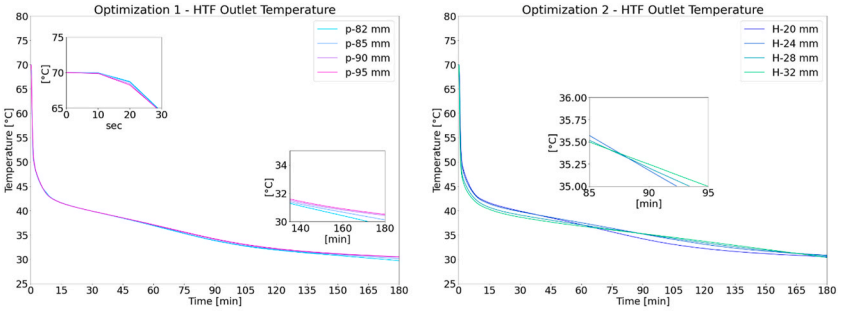

(a) **(b)**

Fig. 13. Comparison of the HTF outlet temperature evolution for optimization 1 (a) and optimization 2 (b).

because of the thermal resistance generated by the advancement of the solidification front inside the PCM. The main difference between the pitch variations is more pronounced after 2 h of operation, as can be observed in Fig. 13a on the right, where a zoom of the last hour of the transient can be observed. The 82 mm pitch shows a rapid drop in the slope of the curve as the closest tube arrangement reduces the path that the solidification front must follow, and the effect of thermal resistance therefore prevails.

Fig. 13b shows the temperature evolution for optimization 2. In this case, the increase in the fin height makes it possible to observe a more stable temperature as *H* increases (from the purple lines to the green lines). The figure illustrates a significant variation in the slope of the curves after about 90 min of discharge, where the configuration with 32 mm of the *H* value shows a gentler slope because the thermal resistance is covered with a higher penetration of the fins length.

3.5.1. *Effects on the melt fraction*

The evolution of the average melt fraction, evaluated as an average value of the θ function in Eq. (3) of the whole volume of the PCM, is shown in Fig. 14 for the two optimizations. The figure illustrates that, for both optimizations, the phase change material reaches complete solidification. The curves show a steeper slope for optimization 1 as the pitch (*p)* varies, as it reduces from 95 mm to 82 mm, and as the height of the fins *(H)* varies, as it increases from 20 mm to 32 mm. All the curves are close together in the first 30 min

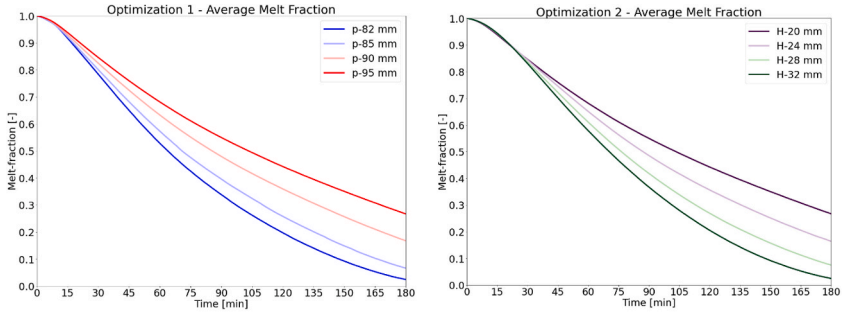

Fig. 14. Comparison of the evolution of the average melt fraction for optimization 1 (a) and optimization 2 (b).

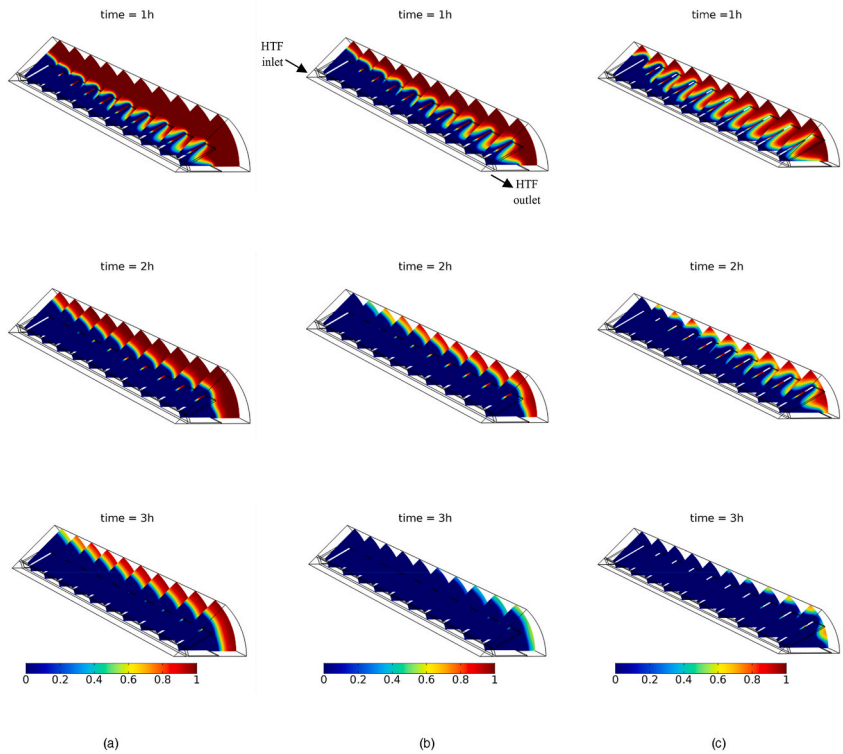

Fig. 15. 3D advancement of the solidification for the initial design configuration with p = 95 mm and H = 20 mm (a), optimized design 1 p = 82 mm and H = 20 mm (b), optimized design 2 p = 95 mm and H = 32 mm (c).

of the discharge, then the curves follow an increasing slope trend as *p* decreases and *H* increases. The trend of the curves confirms that the effect of the proposed solutions, for both optimizations, favours the solidification process of the PCM and its use is maximized within the time frame of 3 h in which the discharge phase must be carried out.

Fig. 15 shows the advancement of the solidification front in the 3D COMSOL simulation model. The blue colour in the map indicates the solid-state, while the red colour indicates the liquid state; the melt fraction was visualized by considering ten cross-sections equally spaced along the tube length after 1, 2, and 3 h of the discharging phase. The HTF enters from the rearmost section and leaves the tube from the front section. The fluid flows at a constant inlet temperature of 25 °C and speeds up the solidification process in the regions of the PCM near the inlet section. Then, as the fluid flows, it extracts latent heat, its temperature increases, and the temperature difference between the HTF and the PCM in turn decreases. As depicted in the figure, the solidification front moves slowly and, after 2 h, the outlet section is in contact with the still liquid PCM, while the PCM is completely solid at the inlet. It can be seen how the moving solid-liquid boundary follows the contours of the metal surface, showing a typical "V" shape [48] between the two fins of the model components, and that this is more pronounced in optimization 2 (Fig. 15c) for the larger fin height value of 32 mm. Fig. 15 (b and c) clearly shows how the proposed optimization solutions increase the velocity of the discharging process over a fixed operation time of 3 h, although the variation in the storage performance, regarding the thermal output power, is acceptable, as previously discussed.

3.5.2. 2D outlet cross-section comparison

A more general visualization of the effects observed in the 3D model is provided in Fig. 16 to help detect the regions of the tube bundle where the PCM is not used in the discharge process. As previously observed, the outer sections of the storage unit are the slowest to complete the discharging phase. Here, the solidification process can be observed for the outlet section of the design case configuration (Fig. 16 (a)), the model with the pitch reduced to 82 mm (Fig. 16 (b)), and the model with the 32 mm height of the fin (Fig. 16 (c)). It is possible to observe how the presence of the finned surfaces positively influences the evolution of the solidification front and modifies the shape of the solid-liquid interface. This effect is more pronounced in the first hour of the discharging, while the configuration of the initial design case (a) has not completed the solidification at the end of the operating time, and still shows a consistent quantity of PCM in the liquid state, which is depicted in the red regions. On the other hand, the liquid PCM has almost disappeared for the optimization 1 and 2 configurations, as can be seen in Fig. 16 b and c.

The analyses carried out to maximize the PCM that completes the solidification process suggest that the configuration which is characterized by the tube pitch reduced to 82 mm and the length of the fins reduced to 20 mm represents an optimal design. Although

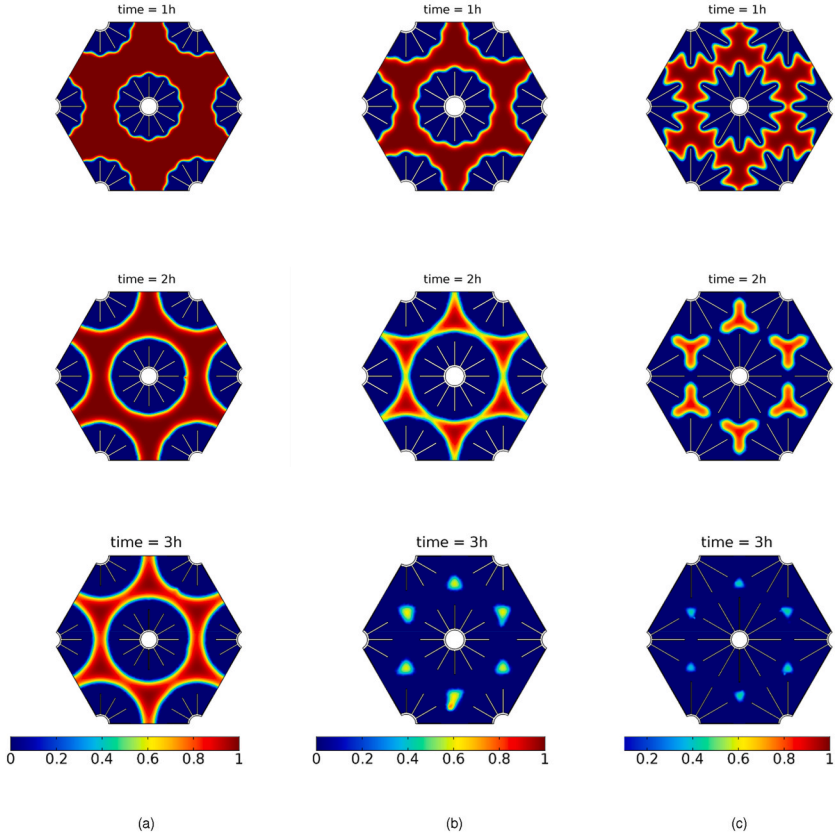

Fig. 16. advancement of the solidification on the outlet cross-section for (a) the initial design configuration with p = 95 mm and H = 20 mm, (b) optimized design 1 with p = 82 mm and H = 20 mm, and (c) optimized design 2 with p = 95 mm and H = 32 mm.

the configuration characterized by a pitch of 95 mm and an increase in the length of the fins to 32 mm showed similar results, in terms of solidified PCM, such a design would require a greater amount of steel (+6.47%), which, in turn, would increase the total costs of the storage unit.

3.6. Load tracking application

The LHTS configuration chosen as the optimal design for the present case study was used for the algorithm applied to evaluate the proposed control strategy. The radiant floor panel profile of the thermal demand that had to be tracked, which is shown in Fig. 11, corresponds to the input of the load tracking algorithm. The profile is characterized by thermal power values that are requested every 15 min; therefore the frequency is dt = 900 s. Moreover, as the LHTS discharging operation takes place in 3 h, from 6:00 to 9:00, there are 13 input parameters and each of them represents the $q^{in,k}$ value at each *k-th* cycle of the algorithm calculations. To locate each point on MAP1, the load tracking algorithm needs to know the HTF**,** Outlet temperature T^k, see Fig. 17.

This value is only known after the first cycle (k = 0) and is equal to 70 °C, which is the initial temperature value of the entire LHTS during the discharge phase. The load tracking algorithm locates the working point of the LHTS on MAP1 with the two parameters $q_{in,k}$ and T^k, and identifies the corresponding load curve, *i*, thus obtaining the relative value of the HTF flow rate with the corresponding inlet velocity $u^{k,i}$. The HTF outlet temperature, T^{k+1}, is calculated for the working points related to the subsequent cycles $(k + 1)$ using MAP2 and moving along identified load curve *i*. Fig. 17 illustrates, with red markers, the 13 working points located by the algorithm on MAP1, where the load curves are depicted for different flow rates. The algorithm selects the load curve for each working point as the one closest to the point and collects the values of the HTF inlet velocity corresponding to the identified load curve. Moreover, all the collected velocities are used to provide the time profile, at a frequency of 15 min, which suggests a flow adjustment of the LHTS according to the thermal demand profile required by the user. An HTF inlet velocity profile is depicted in Fig. 18 with a dashed red line. The bars in Fig. 18 represent the load condition, which is expressed as a percentage of the maximum flow rate and thus as the curves selected for each working point.

The results obtained for the HTF outlet temperature variation were compared with the corresponding temperature values of the COMSOL numerical model to validate the developed load tracking algorithm. The COMSOL numerical model is the same as the one

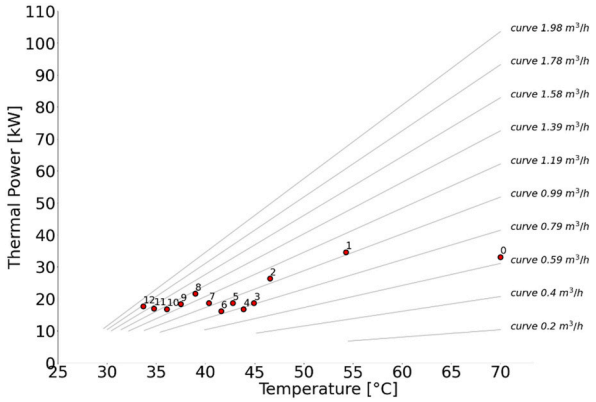

Fig. 17. Working points identified by the algorithm on MAP1 for each *k* cycle.

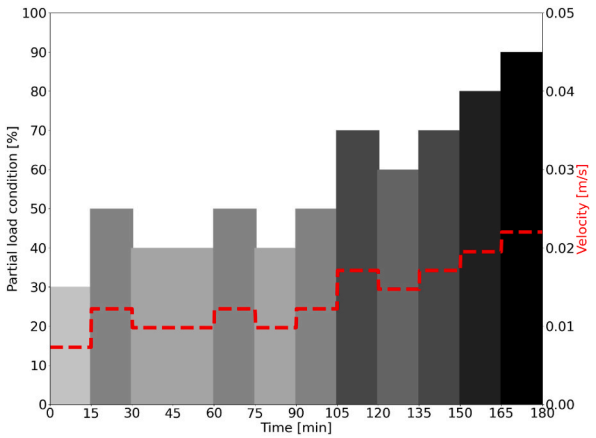

Fig. 18. HTF inlet velocity profile obtained by the algorithm.

that was developed for the 3D elementary module study. Here, the boundary condition for the inlet velocity has been changed. This condition no longer presents a constant value for the entire operating time, and it assumes a variable profile over time. The velocity profile depicted in Fig. 18 is the input of the COMSOL model. In this way, the simulation with a variable inlet velocity could be performed. The numerical model was considered as the reference validation for the algorithm developed in the MATLAB code. This is because the numerical simulation considers the physics of the fluid-tube-PCM concerning the thermal problem by solving the heat diffusion equation at each time step through the finite element method. On the other hand, the load tracking algorithm moves between simulations that have already been performed, which express the storage performance at different load levels. Hence, no thermofluid dynamics equations were introduced and the challenge was to verify the validity of the obtained results by comparing them with those provided by the COMSOL simulation, where all the physics governing equations are accounted for and solved. Fig. 19 shows that there is a close agreement between the algorithm and the COMSOL numerical simulation for both the 10sec and 15min time-step resolutions, as the value of the correlation coefficient (R^2) is 0.987. The mean deviation is about 1.68 °C for the 10 s resolution and the maximum deviation is about 2.93 °C for the 15 min resolution. It can be noted that even when the curves seem to recede (after about 105 min), the trend of the curve provided by the algorithm (blue line) agrees with that shown for the curve obtained from the numerical simulation.

Fig. 20 illustrates the profile of the output power provided by the algorithm. It can be seen how the proposed load tracking model can match the required thermal load, and that there is a maximum deviation of about 1.6 kW. The total energy supply amounts to 61.9 kWh, and it differs, by 0.4 kWh, from the energy required for this application, which is about 62.3 kWh. Furthermore, it is important to point out that these results have been obtained by avoiding a robust and complex numerical model simulation but preserving the validity of the physical problem, as previously discussed concerning the comparison of the temperature evolution curves (see Fig. 19).

4. Conclusions

In this study, the application of a latent thermal storage system with PCM in a building heating system connected to the district heating network has been analysed and the design choices and a feasible control strategy to evaluate the LHTS performance under different operation conditions have been highlighted. The LHTS design consists of a tube bundle heat exchanger with 112 HTF pipes. Twelve longitudinal fins are attached to each of the pipes, the finned tubes are immersed in commercial-grade paraffin, which is used as the PCM, and its optimal configuration has been analysed considering appropriate operational constraints related to the application under study. In the case of district heating, the typical thermal load profile is characterized by a peak power in the early hours of the

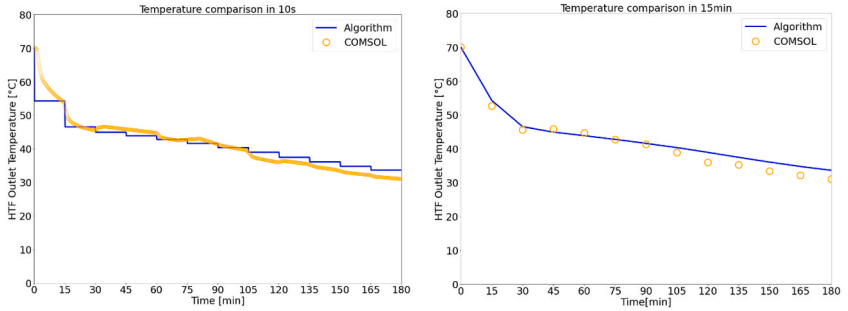

(a) (b)

Fig. 19. Comparison of the HTF outlet temperature profile between the algorithm and numerical model for the 10s frequency (a) and 15-min frequency (b).

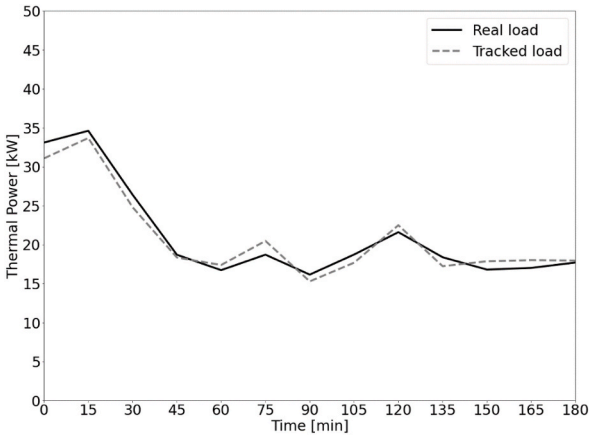

Fig. 20. Thermal power profile obtained for the LHTS by the algorithm to meet the user's demand.

morning. The LHTS integration was designed to reduce this peak demand, which occurs over a defined time frame of approximately 3 h. The LHTS is discharged in the identified time frame. The dynamic thermal behaviour of the LHTS over the 3 h of discharge was evaluated by implementing a 3D numerical model using commercial software based on the finite element scheme. Two design optimization solutions were considered to facilitate the complete solidification of the PCM in 3 h and to ensure the maximum use of the PCM. In this case, 98% of the material filling the storage unit completed the discharge process. The two proposed solutions are characterized by variable fin heights and HTF tube arrangements, depending on the pitch of the tube bundle. In the unit proposed here, the base case, which was designed with 95 mm of pitch and a 20 mm fin height, resulted in PCM solidified amounts of 73.28% after 3 h of discharge, which means the utilization of the phase change material in the system was not optimal. Thus, two optimization solutions were proposed to exploit the maximum PCM utilization over the same discharge time. By decreasing the pitch from 95 mm to 82 mm, 97.56% of the PCM was solidified and provided an increase in the utilization of the PCM of +34%; the same results were obtained by increasing the fin height from 20 mm to 32 mm, whereby 97.52% of the PCM was solidified and its utilization reached +33%, with the same heat transfer surface, phase change volume, and operating conditions as the former optimization solution; these differences justified the slight variation of the average thermal power output. The average thermal power change of ± 3% is an interesting result, since it was achieved by eliminating more than 90% of the PCM that did not contribute to the latent heat exchange in the initial design configuration. In addition, the performed optimization allowed the size and costs of the system to be reduced, without affecting the performance, which was imposed by the thermal application. Optimal integration of the LHTS in a practical application means evaluating the different operating conditions under which the device should work to timely meet the thermal power profile required by the user. For this reason, a control strategy to evaluate the LHTS load modulation was proposed using a simple load tracking algorithm, based on performance maps that correlate the evolution of the HTF outlet temperature over time with the thermal power for different inlet flow rate conditions, to predict the thermal power output of the LHTS. The algorithm can identify the working point of the system during the discharging process, in terms of inlet flow rate profile and HTF outlet temperature, and to adopt an optimal control strategy to match the heating load. The algorithm was validated through the numerical model, which receives the previously obtained flow rate profile as an inlet boundary condition. The validation was conducted by comparing the HTF outlet temperature profiles obtained from the algorithm with those obtained with the numerical model, and a good agreement was observed, with a correlation coefficient of 0.987. The load tracking model was then applied to an existing heating system to reduce the thermal power peak request from the district heating network, that is, to reduce 61.9 kWh of supply, between 6:00 and 9:00 in the morning, to radiant floor panels in an office building located in Turin. The comparison between the measured heating load and the thermal power output of the tracking model showed that the algorithm can match the real power profile, with a maximum deviation of just 1.6 kW. Therefore, the integration of the studied LHTS unit can be considered a feasible solution for the thermal requirements of radiant floor panels. The proposed tracking model is an efficient tool that allows a significant contribution to be made to the analysis of the optimal integrations of a latent thermal storage device in an existing heating system, where a specific thermal power profile is required for thermal applications.

Authors contributions

Andrea Pignata: Conceptualization, Methodology, Software, Validation, Formal analysis, Resources, Data Curation, Writing – Original Draft, Writing – Review & Editing, Visualization. Francesco Demetrio Minuto: Conceptualization, Methodology, Validation, Resources, Writing – Review & Editing, Visualization, Supervision. Andrea Lanzini: Conceptualization, Validation, Resources, Writing – Review & Editing, Visualization, Supervision. Davide Papurello: Conceptualization, Methodology, Validation, Resources, Writing – Review & Editing, Visualization, Supervision, Project administration, Funding acquisition.

Declaration of competing interest

The authors declare that they have no known competing financial interests or personal relationships that could have appeared to influence the work reported in this paper.

Data availability

Data will be made available on request.

References

[1] K.S. Reddy, V. Mudgal, T.K. Mallick, Review of latent heat thermal energy storage for improved material stability and effective load management, J. Energy Storage 15 (2018) 205–227, https://doi.org/10.1016/j.est.2017.11.005.
[2] V. Verda, F. Colella, Primary energy savings through thermal storage in district heating networks, Energy (2011), https://doi.org/10.1016/j.energy.2011.04.015.
[3] I. Dinçer, M.A. Rosen, Thermal Energy Storage: Systems and Applications, second ed., 2010, https://doi.org/10.1002/9780470970751.
[4] A. Abhat, Low temperature latent heat thermal energy storage: heat storage materials, Sol. Energy 30 (1983) 313–332, https://doi.org/10.1016/0038-092X(83)90186-X.
[5] B. Zalba, J.M. Marín, L.F. Cabeza, H. Mehling, Review on thermal energy storage with phase change: materials, heat transfer analysis and applications, Appl. Therm. Eng. 23 (2003) 251–283, https://doi.org/10.1016/S1359-4311(02)00192-8.
[6] A. Sharma, V. V Tyagi, C.R. Chen, D. Buddhi, Review on Thermal Energy Storage with Phase Change Materials and Applications, Renewable and Sustainable Energy Reviews, 2009, https://doi.org/10.1016/j.rser.2007.10.005.
[7] M. Farid, A. Auckaili, S.A. Khateeb Razack, S. Al-Hallaj, A review on phase change energy storage: materials and applications, Energy Convers. Manag. 45 (2004) 1597–1615, https://doi.org/10.1016/j.enconman.2003.09.015.

[8] K. Du, J. Calautit, Z. Wang, Y. Wu, H. Liu, A review of the applications of phase change materials in cooling, heating and power generation in different temperature ranges, Appl. Energy 220 (2018) 242–273, https://doi.org/10.1016/j.apenergy.2018.03.005.

[9] T. Hai, A. Abidi, J.M. Zain, S.M. Sajadi, M.Z. Mahmoud, H.Ş. Aybar, Assessment of using solar system enhanced with MWCNT in PCM-enhanced building to decrease thermal energy usage in ejector cooling system, J. Build. Eng. 55 (2022), 104697, https://doi.org/10.1016/j.jobe.2022.104697.

[10] S. Alotaibi, M. Alhuyi Nazari, District cooling in the Middle East & North Africa; history, current status, and future opportunities, J. Build. Eng. (2023), 107522, https://doi.org/10.1016/j.jobe.2023.107522.

[11] T. Hai, A. Abidi, L. Wang, A.M. Abed, M.Z. Mahmoud, E.M. Tag El Din, G.F. Smaisim, Simulation of solar thermal panel systems with nanofluid flow and PCM for energy consumption management of buildings, J. Build. Eng. 58 (2022), 104981, https://doi.org/10.1016/j.jobe.2022.104981.

[12] S.A. Khawaja, S.A. Memon, Novel indicators to evaluate PCM performance under different ventilation strategies by considering the impact of climate change, J. Build. Eng. 74 (2023), 106848, https://doi.org/10.1016/j.jobe.2023.106848.

[13] J. Hu, X. Wang, W. Chen, Y. Yin, Y. Li, OPV-PCM-ETFE foils in use for public buildings: electrical performance and thermal characteristics, J. Build. Eng. 71 (2023), 106427, https://doi.org/10.1016/j.jobe.2023.106427.

[14] J. Mustafa, S. Alqaed, M. Sharifpur, PCM embedded radiant chilled ceiling as a solution to shift the cooling peak load-focusing on solidification process acceleration, J. Build. Eng. 57 (2022), 104894, https://doi.org/10.1016/j.jobe.2022.104894.

[15] R.I. Hatamleh, N.H. Abu-Hamdeh, R.A.R. Bantan, Integration of a solar air heater to a building equipped with PCM to reduce the energy demand, J. Build. Eng. 48 (2022), 103948, https://doi.org/10.1016/j.jobe.2021.103948.

[16] N.H. Abu-Hamdeh, R.A. Alsulami, R.I. Hatamleh, A case study in the field of building sustainability energy: performance enhancement of solar air heater equipped with PCM: a trade-off between energy consumption and absorbed energy, J. Build. Eng. 48 (2022), 103903, https://doi.org/10.1016/j.jobe.2021.103903.

[17] A. Saxena, E. Cuce, D.B. Singh, M. Sethi, P.M. Cuce, A.A. Sagade, A. Kumar, Experimental studies of latent heat storage based solar air heater for space heating: a comparative analysis, J. Build. Eng. 69 (2023), 106282, https://doi.org/10.1016/j.jobe.2023.106282.

[18] C. Shi, Q. Zhao, P. Wang, L. Yang, Preparation, performance study and application simulation of gypsum-paraffin/EG composite phase change building wallboard, J. Build. Eng. 65 (2023), 105813, https://doi.org/10.1016/j.jobe.2022.105813.

[19] P. Devaux, M.M. Farid, Benefits of PCM underfloor heating with PCM wallboards for space heating in winter, Appl. Energy 191 (2017) 593–602, https://doi.org/10.1016/j.apenergy.2017.01.060.

[20] Y. Cao, I.B. Mansir, A. Mouldi, F. Aouaini, S.M. Bouzgarrou, R. Marzouki, M. Dahari, M. Wae-hayee, A. Mohamed, Designing a system for battery thermal management: cooling LIBs by nano-encapsulated phase change material, Case Stud. Therm. Eng. 33 (2022), 101943, https://doi.org/10.1016/j.csite.2022.101943.

[21] A. Mitra, R. Kumar, D.K. Singh, Z. Said, Advances in the improvement of thermal-conductivity of phase change material-based lithium-ion battery thermal management systems: an updated review, J. Energy Storage 53 (2022), 105195, https://doi.org/10.1016/j.est.2022.105195.

[22] L. Kalapala, J.K. Devanuri, Influence of operational and design parameters on the performance of a PCM based heat exchanger for thermal energy storage – a review, J. Energy Storage 20 (2018) 497–519, https://doi.org/10.1016/j.est.2018.10.024.

[23] P.B. Salunkhe, P.S. Shembekar, A Review on Effect of Phase Change Material Encapsulation on the Thermal Performance of a System, Renewable and Sustainable Energy Reviews, 2012, https://doi.org/10.1016/j.rser.2012.05.037.

[24] Y. Lin, Y. Jia, G. Alva, G. Fang, Review on thermal conductivity enhancement, thermal properties and applications of phase change materials in thermal energy storage, Renew. Sustain. Energy Rev. 82 (2018) 2730–2742, https://doi.org/10.1016/j.rser.2017.10.002.

[25] M. Sheikholeslami, Efficacy of porous foam on discharging of phase change material with inclusion of hybrid nanomaterial, J. Energy Storage 62 (2023), 106925, https://doi.org/10.1016/j.est.2023.106925.

[26] G. Triscari, M. Santovito, M. Bressan, D. Papurello, Experimental and model validation of a phase change material heat exchanger integrated into a real building, Int. J. Energy Res. 45 (2021) 18222–18236, https://doi.org/10.1002/er.7037.

[27] H. Alqahtani, M.M. Selim, Passive techniques for improvement of freezing within storage system involving nanoparticles, J. Energy Storage 70 (2023), 107870, https://doi.org/10.1016/j.est.2023.107870.

[28] S. Jegadheeswaran, S.D. Pohekar, Performance Enhancement in Latent Heat Thermal Storage System: A Review, Renewable and Sustainable Energy Reviews, 2009, https://doi.org/10.1016/j.rser.2009.06.024.

[29] F. Agyenim, N. Hewitt, P. Eames, M. Smyth, A review of materials, heat transfer and phase change problem formulation for latent heat thermal energy storage systems (LHTESS), Renew. Sustain. Energy Rev. 14 (2010) 615–628, https://doi.org/10.1016/j.rser.2009.10.015.

[30] J. Wołoszyn, K. Szopa, G. Czerwiński, Enhanced heat transfer in a PCM shell-and-tube thermal energy storage system, Appl. Therm. Eng. 196 (2021), 117332, https://doi.org/10.1016/j.applthermaleng.2021.117332.

[31] H. Liang, J. Niu, Y. Gan, Performance optimization for shell-and-tube PCM thermal energy storage, J. Energy Storage 30 (2020), 101421, https://doi.org/10.1016/j.est.2020.101421.

[32] M.Y. Yazici, M. Avci, O. Aydin, M. Akgun, On the Effect of Eccentricity of a Horizontal Tube-In-Shell Storage Unit on Solidification of a PCM, Applied Thermal Engineering, 2014, https://doi.org/10.1016/j.applthermaleng.2013.12.005.

[33] Z. Li, Z.G. Wu, Analysis of HTFs, PCMs and fins effects on the thermal performance of shell-tube thermal energy storage units, Sol. Energy 122 (2015) 382–395, https://doi.org/10.1016/j.solener.2015.09.019.

[34] T. Barz, J. Emhofer, Paraffins as phase change material in a compact plate-fin heat exchanger - Part I: experimental analysis and modeling of complete phase transitions, J. Energy Storage 33 (2021), 102128, https://doi.org/10.1016/j.est.2020.102128.

[35] S. Wu, Y. Huang, C. Zhang, Y. Chen, Role of tree-shaped fins in charging performance of a latent heat storage unit, Int. J. Energy Res. 44 (2020) 4800–4811, https://doi.org/10.1002/er.5268.

[36] A. Sciacovelli, F. Gagliardi, V. Verda, Maximization of performance of a PCM latent heat storage system with innovative fins, Appl. Energy 137 (2015) 707–715, https://doi.org/10.1016/j.apenergy.2014.07.015.

[37] A.M. Abdulateef, S. Mat, J. Abdulateef, K. Sopian, A.A. Al-Abidi, Geometric and design parameters of fins employed for enhancing thermal energy storage systems: a review, Renew. Sustain. Energy Rev. 82 (2018) 1620–1635, https://doi.org/10.1016/j.rser.2017.07.009.

[38] M. Fallah Najafabadi, M. Farhadi, H. Talebi Rostami, Numerically analysis of a Phase-change Material in concentric double-pipe helical coil with turbulent flow as thermal storage unit in solar water heaters, J. Energy Storage 55 (2022), 105712, https://doi.org/10.1016/j.est.2022.105712.

[39] M.A. Kibria, M.R. Anisur, M.H. Mahfuz, R. Saidur, I.H.S.C. Metselaar, Numerical and experimental investigation of heat transfer in a shell and tube thermal energy storage system, Int. Commun. Heat Mass Tran. (2014), https://doi.org/10.1016/j.icheatmasstransfer.2014.02.023.

[40] W. Youssef, Y.T. Ge, S.A. Tassou, CFD modelling development and experimental validation of a phase change material (PCM) heat exchanger with spiral-wired tubes, Energy Convers. Manag. 157 (2018) 498–510, https://doi.org/10.1016/j.enconman.2017.12.036.

[41] D. Groulx, W. Ogoh, Solid-liquid phase change simulation applied to a cylindrical latent heat energy storage system, Proc. 5th Annual COMSOL Conf. (2009) 7.

[42] X. Yang, Z. Lu, Q. Bai, Q. Zhang, L. Jin, J. Yan, Thermal performance of a shell-and-tube latent heat thermal energy storage unit: role of annular fins, Appl. Energy 202 (2017) 558–570, https://doi.org/10.1016/j.apenergy.2017.05.007.

[43] S. Tiari, S. Qiu, Three-dimensional simulation of high temperature latent heat thermal energy storage system assisted by finned heat pipes, Energy Convers. Manag. 105 (2015) 260–271, https://doi.org/10.1016/j.enconman.2015.08.004.

[44] J. Yang, X. Du, L. Yang, Y. Yang, Numerical analysis on the thermal behavior of high temperature latent heat thermal energy storage system, Sol. Energy 98 (2013) 543–552, https://doi.org/10.1016/j.solener.2013.10.028.

[45] K.A.R. Ismail, C.L.F. Alves, M.S. Modesto, Numerical and experimental study on the solidification of PCM around a vertical axially finned isothermal cylinder, Appl. Therm. Eng. 21 (2001) 53–77, https://doi.org/10.1016/S1359-4311(00)00002-8.

[46] A. Castell, C. Solé, M. Medrano, J. Roca, L.F. Cabeza, D. García, Natural convection heat transfer coefficients in phase change material (PCM) modules with external vertical fins, Appl. Therm. Eng. 28 (2008) 1676–1686, https://doi.org/10.1016/j.applthermaleng.2007.11.004.

[47] M.K. Rathod, J. Banerjee, Thermal performance enhancement of shell and tube Latent Heat Storage Unit using longitudinal fins, Appl. Therm. Eng. 75 (2015) 1084–1092, https://doi.org/10.1016/j.applthermaleng.2014.10.074.
[48] M.J. Hosseini, A.A. Ranjbar, M. Rahimi, R. Bahrampoury, Experimental and numerical evaluation of longitudinally finned latent heat thermal storage systems, Energy Build. 99 (2015) 263–272, https://doi.org/10.1016/j.enbuild.2015.04.045.
[49] F. Agyenim, P. Eames, M. Smyth, A comparison of heat transfer enhancement in a medium temperature thermal energy storage heat exchanger using fins, Sol. Energy 83 (2009) 1509–1520, https://doi.org/10.1016/j.solener.2009.04.007.
[50] H. Niyas, S. Prasad, P. Muthukumar, Performance investigation of a lab–scale latent heat storage prototype – numerical results, Energy Convers. Manag. 135 (2017) 188–199, https://doi.org/10.1016/j.enconman.2016.12.075.
[51] B.G. Abreha, P. Mahanta, G. Trivedi, Performance investigation of lab-scale shell and tube LHS prototype, J. Energy Storage (2020), https://doi.org/10.1016/j.est.2020.101527.
[52] Z. Khan, Z. Khan, K. Tabeshf, Parametric investigations to enhance thermal performance of paraffin through a novel geometrical configuration of shell and tube latent thermal storage system, Energy Convers. Manag. 127 (2016) 355–365, https://doi.org/10.1016/j.enconman.2016.09.030.
[53] F. Agyenim, N. Hewitt, The development of a finned phase change material (PCM) storage system to take advantage of off-peak electricity tariff for improvement in cost of heat pump operation, Energy Build. (2010), https://doi.org/10.1016/j.enbuild.2010.03.027.
[54] N. Nallusamy, R. Velraj, Numerical and experimental investigation on a combined sensible and latent heat storage unit integrated with solar water heating system, J. Solar Energy Eng., Transact. ASME (2009), https://doi.org/10.1115/1.3197600.
[55] Y. Li, N. Zhang, Z. Ding, Investigation on the energy performance of using air-source heat pump to charge PCM storage tank, J. Energy Storage (2020), https://doi.org/10.1016/j.est.2020.101270.
[56] T. Xu, E.N. Humire, J.N.W. Chiu, S. Sawalha, Numerical Thermal Performance Investigation of a Latent Heat Storage Prototype toward Effective Use in Residential Heating Systems, Applied Energy, 2020, https://doi.org/10.1016/j.apenergy.2020.115631.
[57] A. Sciacovelli, V. Verda, F. Gagliardi, Thermo-fluid dynamic model for control analysis of latent heat thermal storage system, proceedings of the 25th international conference on efficiency, cost, optimization and simulation of energy conversion systems and processes, ECOS 2012 1 (2012) 321–333.
[58] A. Colangelo, E. Guelpa, A. Lanzini, G. Mancò, V. Verda, Compact model of latent heat thermal storage for its integration in multi-energy systems, Appl. Sci. 10 (2020), https://doi.org/10.3390/app10248970, 1–14.
[59] E. Guelpa, Impact of thermal masses on the peak load in district heating systems, Energy 214 (2020), 118849, https://doi.org/10.1016/j.energy.2020.118849.
[60] LuisaF. Cabeza, H. Mehling, Heat and Cold Storage with PCM. An up to Date Introduction into Basics and Applications - Publisher:Springer, Heat and Mass Transfer, 2008, ISBN 978-3-540-68557-9.
[61] A. Hasan, Phase change material energy storage system employing palmitic acid, Sol. Energy 52 (1994) 143–154, https://doi.org/10.1016/0038-092X(94)90064-7.
[62] Reynolds' Number - an overview | ScienceDirect Topics, (n.d.). https://www.sciencedirect.com/topics/engineering/reynolds-number (accessed December 12, 2022).
[63] S. Kuravi, K.M. Kota, J. Du, L.C. Chow, Numerical investigation of flow and heat transfer performance of nano-encapsulated phase change material slurry in microchannels, J. Heat Tran. (2009), https://doi.org/10.1115/1.3084123.
[64] H. Yang, Y. He, Solving heat transfer problems with phase change via smoothed effective heat capacity and element-free Galerkin methods, Int. Commun. Heat Mass Tran. (2010), https://doi.org/10.1016/j.icheatmasstransfer.2009.12.002.
[65] W. Ogoh, D. Groulx, Effects of the Heat Transfer Fluid Velocity on the Storage Characteristics of a Cylindrical Latent Heat Energy Storage System: A Numerical Study, Heat and Mass Transfer/Waerme- Und Stoffuebertragung, 2012, https://doi.org/10.1007/s00231-011-0888-3.
[66] Simulating phase change heat transfer using Comsol and Fluent: effect of the mushy - zone constant - computational Thermal Sciences, Int. J. 7 (5–6) (2015). Begell House Digital Library, (n.d.), https://www.dl.begellhouse.com/journals/648192910890cd0e,4860a26f63ba7840,7f0c2645687fec74.html. (Accessed 15 December 2022).
[67] PureTemp 53 technical data sheet, (n.d.). http://www.puretemp.com/stories/puretemp-53-tds (accessed April 22, 2021).
[68] D. Papurello, V. Vitulli, F. Minuto, L. Bottaccioli, A. Lanzini, R. Borchiellini, Strategies for demand-side management in an office building integrated with rooftop façade PV installations, IJES 63 (2019) 311–314, https://doi.org/10.18280/ti-ijes.632-428.